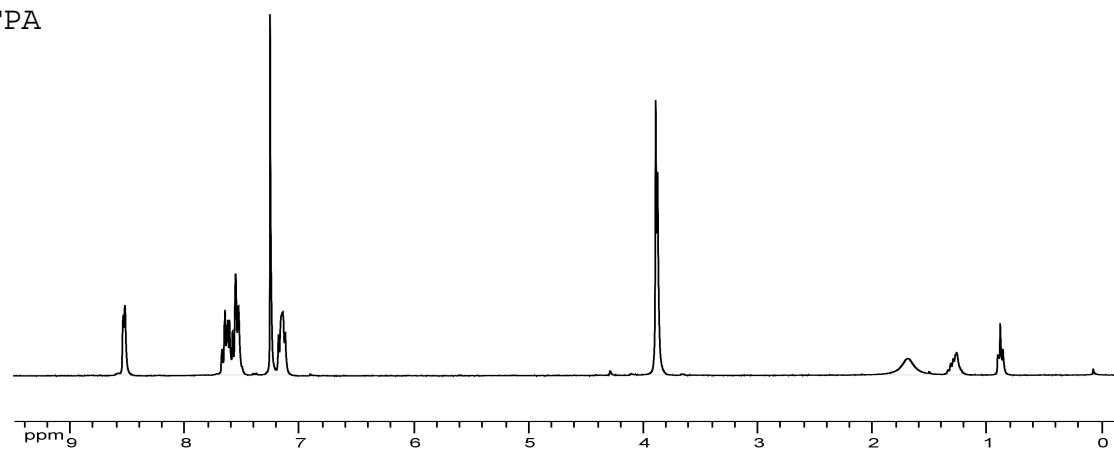
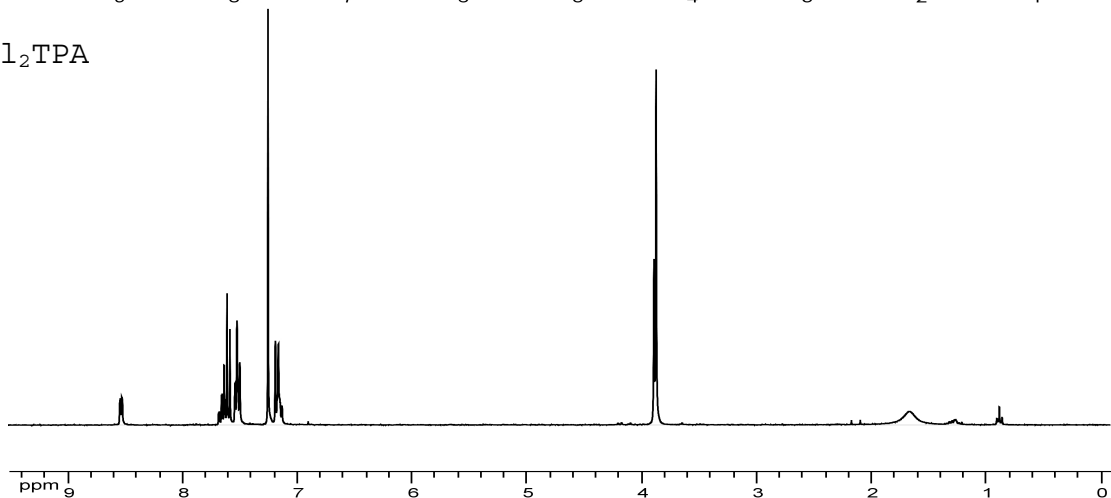


Supporting Information

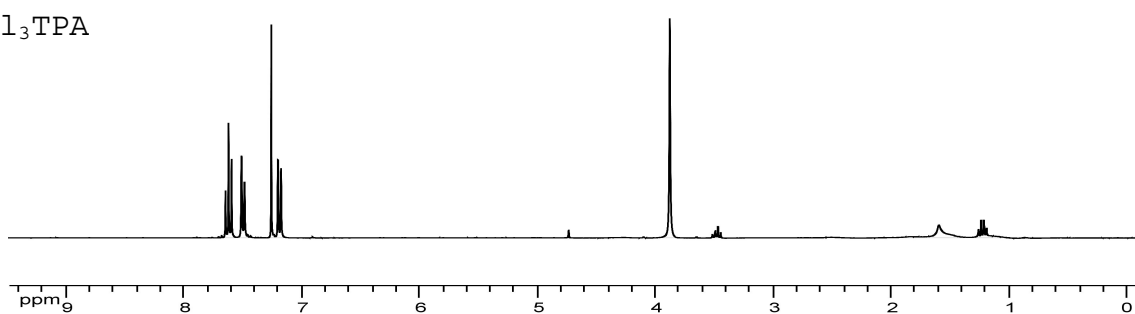
Cl₁TPA



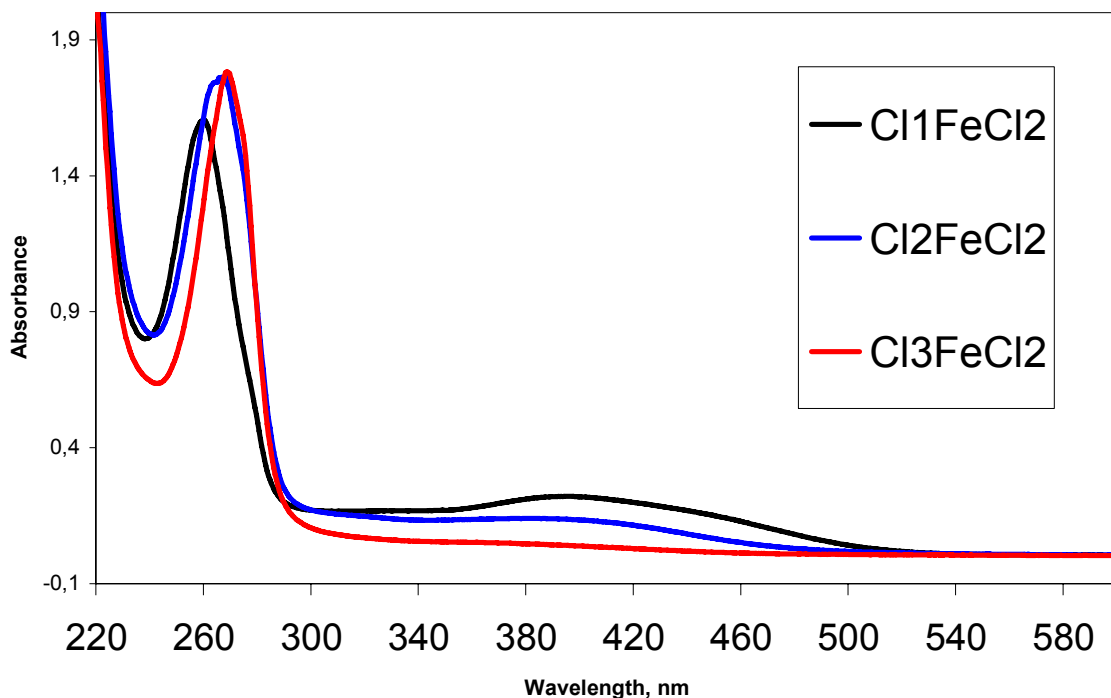
Cl₂TPA



Cl₃TPA



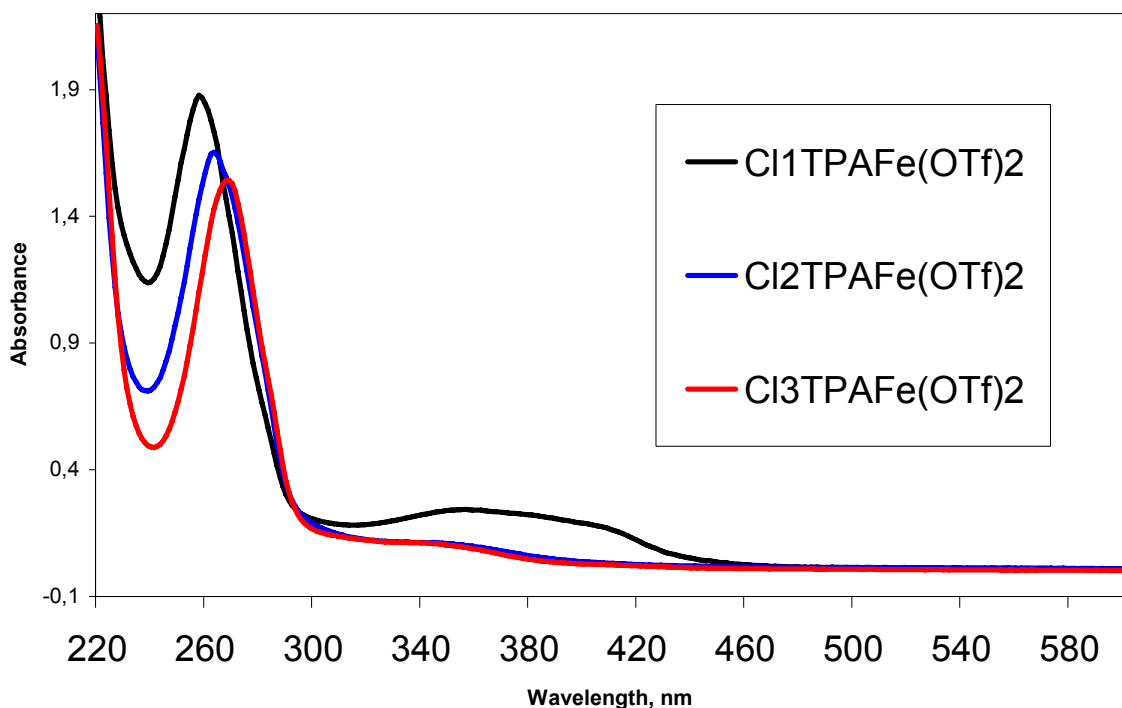
S.I. 0: ¹H NMR spectrum of the ligands Cl₁TPA, Cl₂TPA, and Cl₃TPA, in CDCl₃.



	Cl ₁ TPAFeCl ₂	Cl ₂ TPAFeCl ₂	Cl ₃ TPAFeCl ₂
$\pi = > \pi^*$	259 (8.3)	267 (9.4)	269 (13.3)
MLCT	392 (1.2)	373 (0.6)	/

Wavelengths in nm, (molecular extinction coefficients in mol⁻¹.cm²)

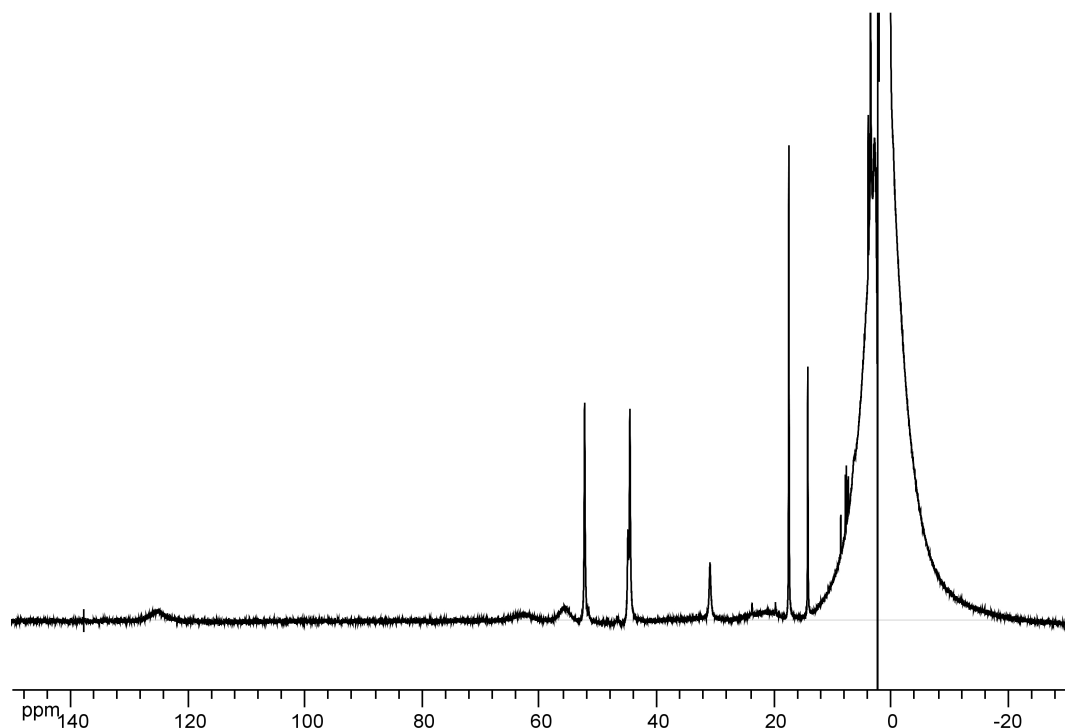
S.I. 1: Normalized UV-vis. traces of the new Cl₁₋₃TPAFeCl₂ compounds, and numerical data.



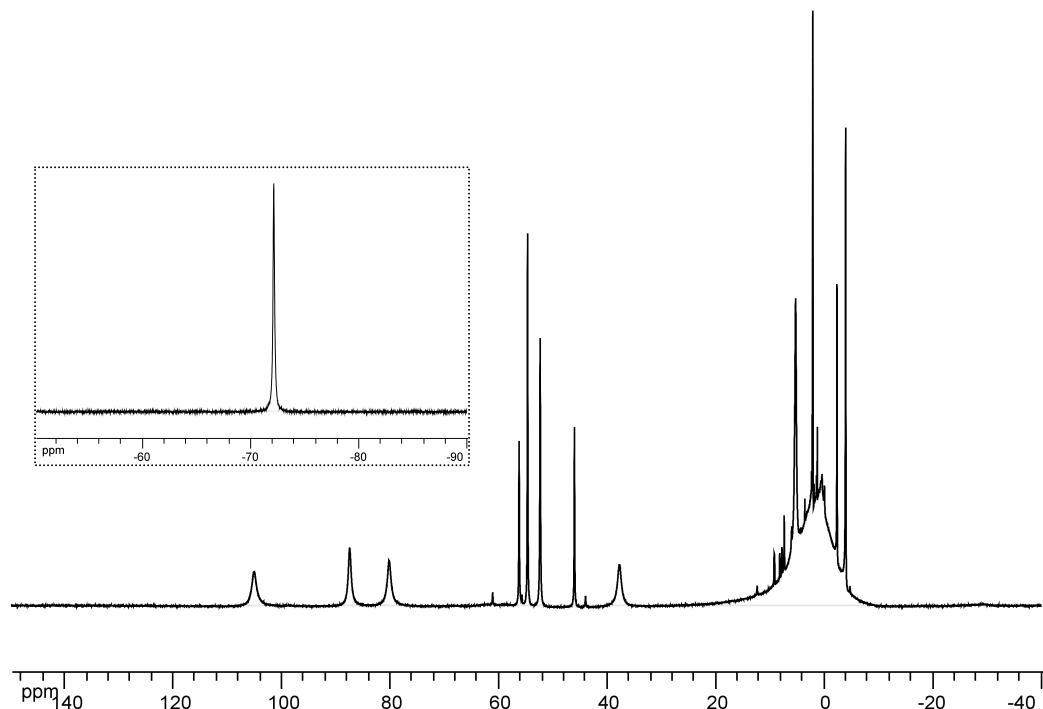
	$\text{Cl}_1\text{TPAFe}(\text{OTf})_2$	$\text{Cl}_2\text{TPAFe}(\text{OTf})_2$	$\text{Cl}_3\text{TPAFe}(\text{OTf})_2$
$\pi = \pi^*$	258 (10.2)	264 (8.5)	268 (9.4)
MLCT	354 (1.3), 415 (sh.)	351 (0.6)	344 (0.6)

Wavelengths in nm, (molecular extinction coefficients in $\text{mol}^{-1} \cdot \text{cm}^2$)

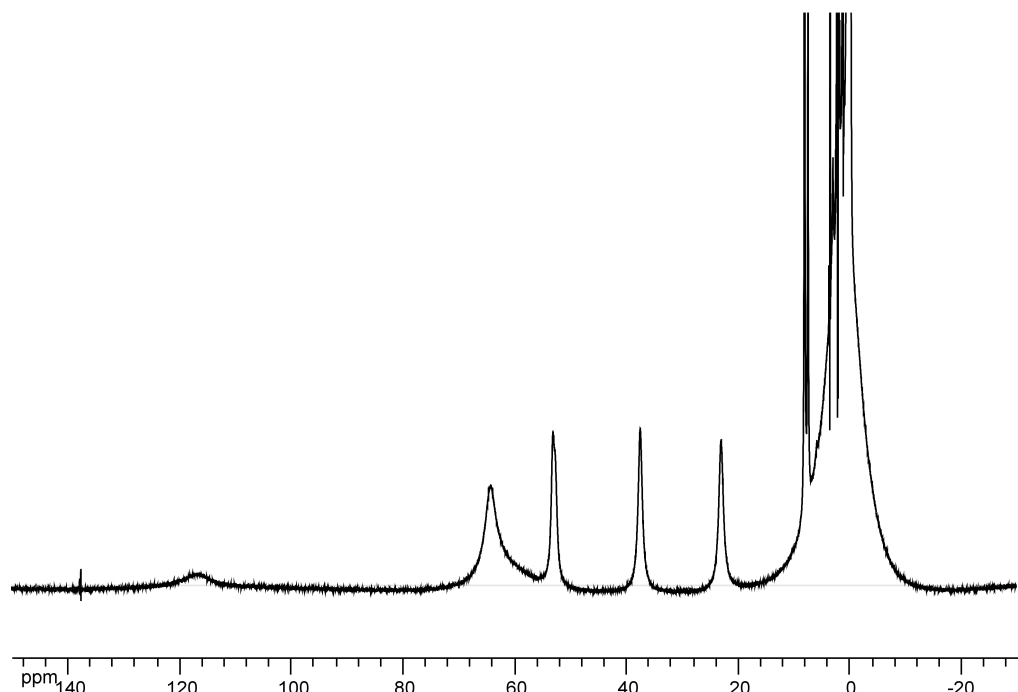
S.I. 2: Normalized UV-vis. traces of the new $\text{Cl}_{1-3}\text{TPAFe}(\text{OTf})_2$ compounds, and numerical data.



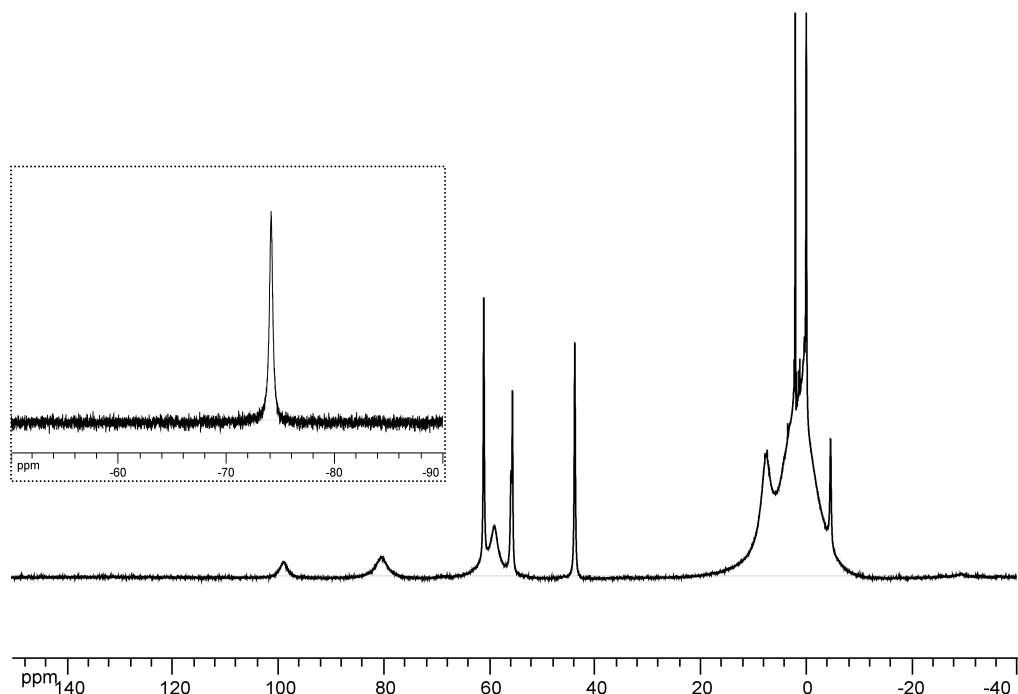
S.I. 3a: ¹H NMR spectrum of complex Cl₁FeCl₂ in CD₃CN, R.T.



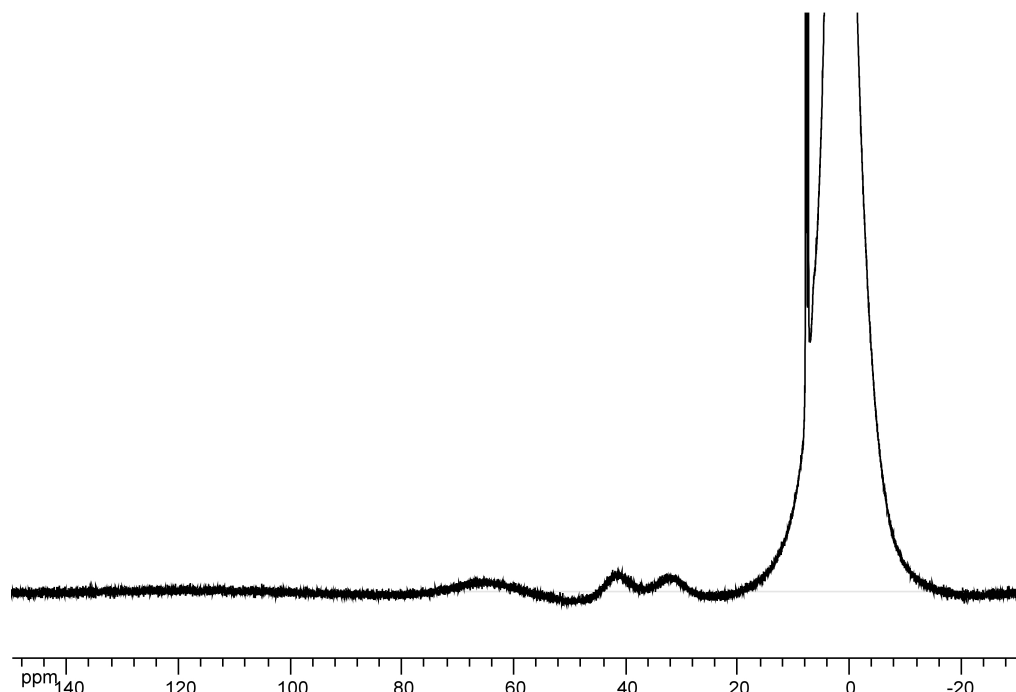
S.I. 3b: ¹H NMR spectrum of complex Cl₁Fe(OTf)₂ dissolved in CD₃CN, R.T. Insert: ¹⁹F NMR in CD₃CN.



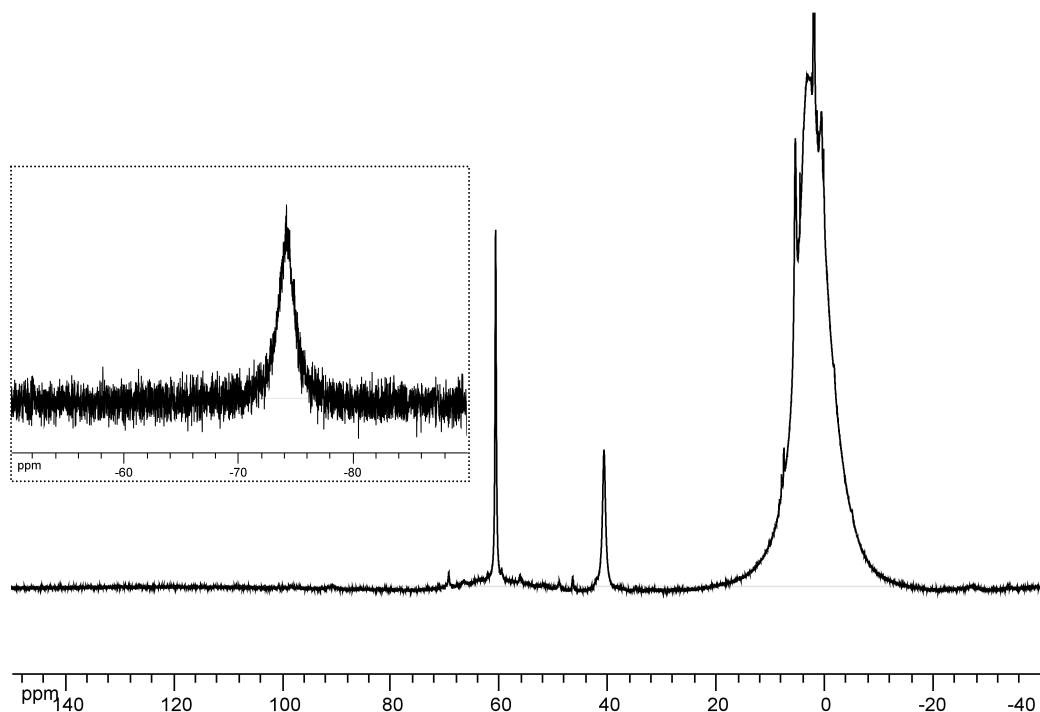
S.I. 4a: ¹H NMR spectrum of complex Cl_2FeCl_2 in CD_3CN , R.T.



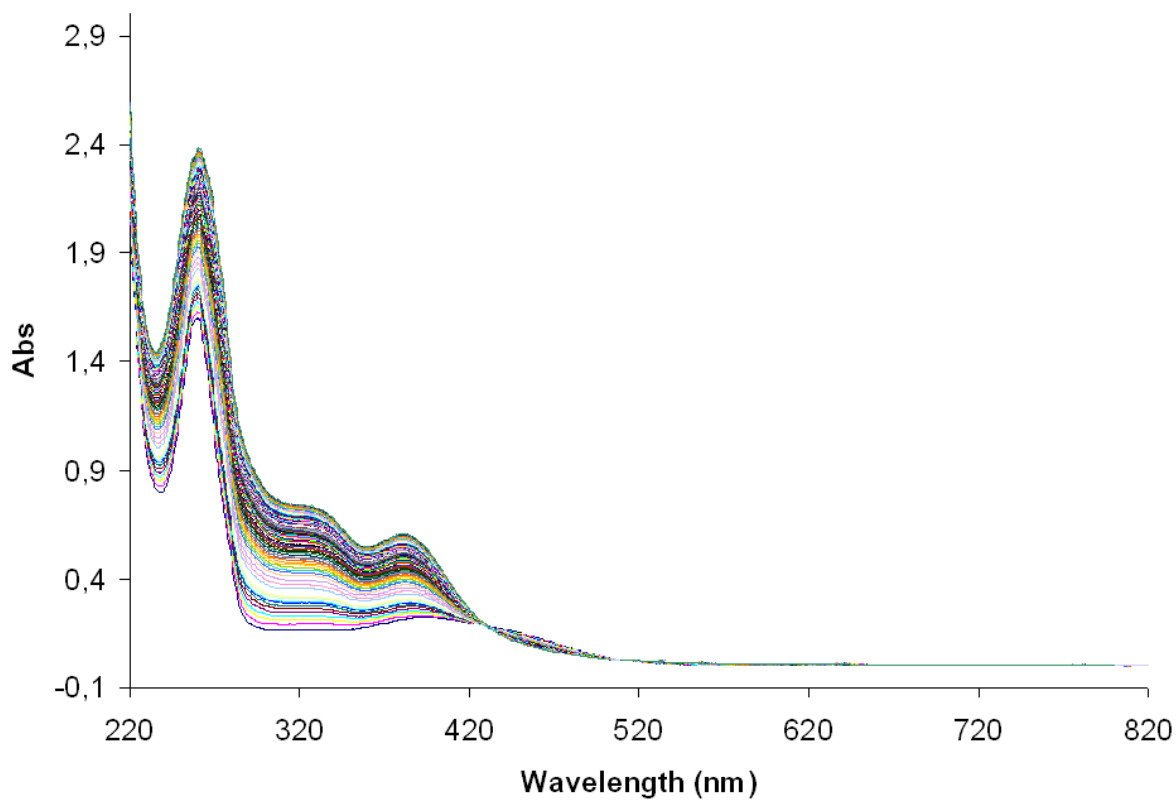
S.I. 4b: ¹H NMR spectrum of complex $\text{Cl}_2\text{Fe}(\text{OTf})_2$ dissolved in CD_3CN , R.T. Insert: ¹⁹F NMR in CD_3CN .



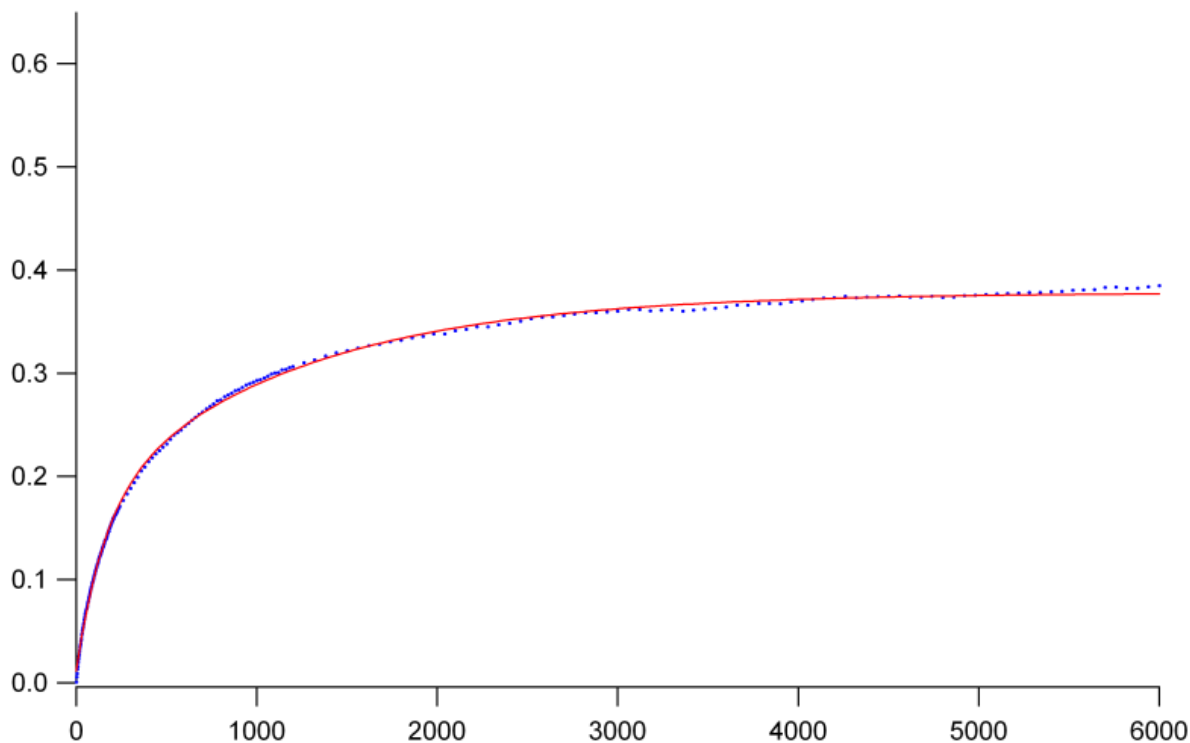
S.I. 5a: ¹H NMR spectrum of complex Cl₃FeCl₂ in CD₃CN, R.T.



S.I. 5b: ¹H NMR spectrum of complex Cl₃Fe(OTf)₂ dissolved in CD₃CN, R.T. Insert: ¹⁹F NMR in CD₃CN.



S.I. 6: Spectral absorption changes versus time for oxygenation of $\text{Cl}_1\text{TPAFeCl}_2$, at room temperature in CH_3CN under O_2 -saturated atmosphere. Conditions: one scan every 10 minutes for two hours, then every hour for three days.

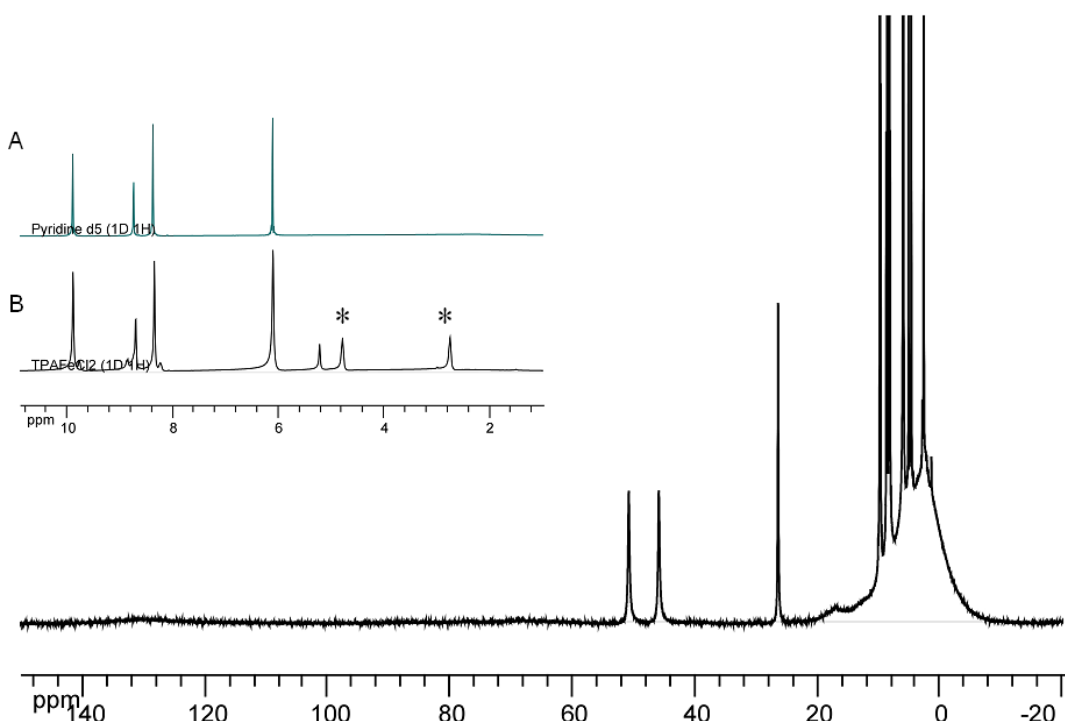


S.I. 7: Y/X scale : Abs *versus* time (min).

Variation of absorbance at a single wavelength (380 nm) of $\text{Cl}_1\text{TPAFeCl}_2$ in CH_3CN under O_2 -saturated atmosphere (see S.I. 6). Experimental points: blue dots. Reactivity of $\text{Cl}_1\text{TPAFeCl}_2$ with O_2 occurred within two kinetically-distinct steps (see reference 18 in text) quantified by fitting (red trace) experimental data, using the following function:

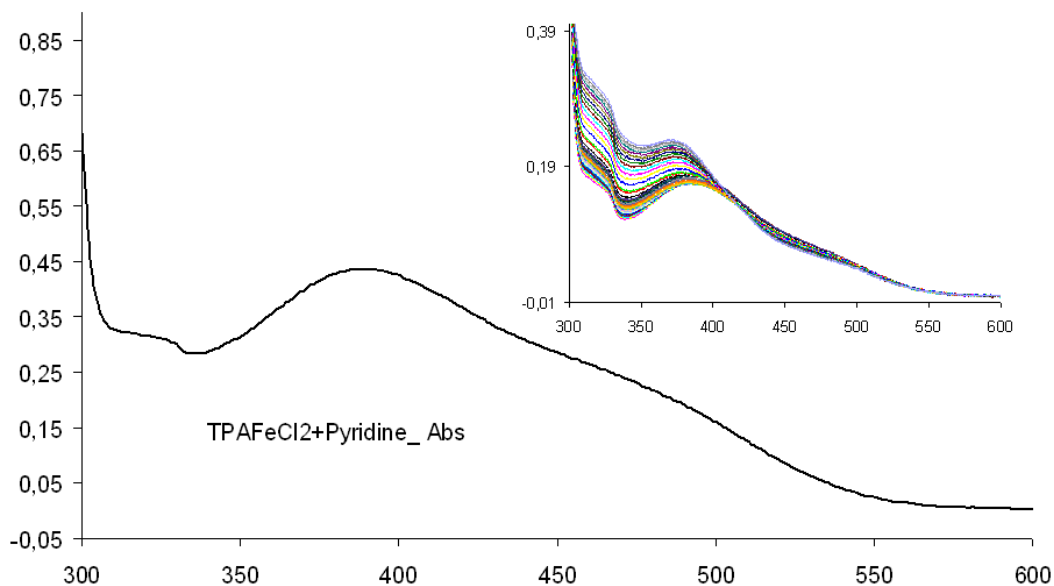
$$f(t) = A_0 + A_1 \exp^{-k_1 t} + A_2 \exp^{-k_2 t}$$

final values: $A_0 = 0.37815 \pm 0.000583$
 $A_1 = 0.15533 \pm 0.00268$
 $A_2 = 0.021113 \pm 0.00256$
 $k_1 = 0.0064276 \pm 0.000147 \text{ mn}^{-1}$
 $k_2 = 0.00086632 \pm 0.0000164 \text{ mn}^{-1}$



S.I. 8: ^1H NMR spectrum of TPAFeCl_2 in d_5 pyridine, demonstrating the high-spin state of the metal even in pyridine. A similar spectrum is obtained in CD_3CN [see: D. Mandon; A. Machkour; S. Goetz; R. Welter, *Inorg. Chem.*, **2002**, *41*, 5363 – 5372, and L. Benhamou; M. Lachkar; D. Mandon; R. Welter, *Dalton Trans.*, **2008**, 6996 – 7003]. Insert: diamagnetic region. A, spectrum of d_5 pyridine (pure solvent, for comparison purpose); B, spectrum of TPAFeCl_2 . The asterisks denote the presence of small amounts of diethyl ether, which appears at these frequencies in d_5 pyridine.

No change occurs upon addition of small amounts of acetic acid in the medium.



S.I. 9: UV-visible spectrum of TPAFeCl₂ in pyridine. The MLCT band at $\lambda = 389$ nm and 472 nm (shoulder) is shifted by comparison with the $\lambda = 427$ nm absorption measured in CH₃CN. No change occurs upon addition of small amounts of acetic acid in the medium. Insert: smooth conversion into the μ -oxo diferric derivative in pyridine.

To be compared with data obtained in CH₃CN and reported in: N. K. Thallaj; O. Rotthaus; L. Benhamou; N. Humbert; M. Elhabiri; M. Lachkar; R. Welter; A.-M. Albrecht-Gary; D. Mandon, *Chem. Eur. J.*, 2008, 14, 6742 – 6753.